TUTORIAL/ARTICLE DIDACTIQUE

The rotating-saddle trap: a mechanical analogy to RF-electric-quadrupole ion trapping?

R.I. Thompson, T.J. Harmon, and M.G. Ball

Abstract: The rotating-saddle potential ball-bearing trap has long been used as a mechanical analogue to explain the operating principles of the Paul-type RF-electric-quadrupole ion trap. This paper outlines the shortcomings of this analogy, as well as explaining how and why this system remains an excellent tool for explaining ion-trap operation. The basic theory of the operating principles of the rotating-saddle trap is provided, which, unlike the Paul Trap is analytically solvable in the friction-free regime. In addition, some extensions to this theory are presented to examine such effects as friction. These results are compared with the equivalent results for Paul-Trap theory, as well as to experimental results measured with a rotating-saddle trap constructed at the University of Calgary. The technical details of this trap, an excellent tool for either lecture demonstrations or teaching laboratory experiments, are also presented, as well as some comments on building such a trap.

PACS Nos.: 45.50-j, 01.50Pa, 32.80Pj

Résumé : Le piège mécanique pour bille dure avec potentiel en selle tournante a longtemps été utilisé comme analogue mécanique pour expliquer le fonctionnement du piège ionique à quadripôle électrique RF de Paul. Nous soulignons ici les faiblesses de cette analogie, tout en expliquant comment et pourquoi ce système demeure un excellent outil pour expliquer le fonctionnement des pièges ioniques. Nous énonçons la théorie de base décrivant le fonctionnement du potentiel en selle tournante qui, contrairement au piège de Paul, a une solution analytique en régime sans friction. Nous présentons aussi des généralisations de cette théorie pour examiner certains effets comme la friction. Nous comparons nos résultats avec des résultats équivalents pour un piège de Paul, ainsi qu'avec des mesures prises sur un piège à selle tournante construit à l'Université de Calgary. Nous expliquons comment le construire et présentons les détails techniques de ce piège, un excellent outil pour des démonstrations en classe et au laboratoire d'enseignement.

[Traduit par la Rédaction]

R.I. Thompson,[1] T.J. Harmon, and M.G. Ball. Department of Physics and Astronomy, The University of Calgary, 2500 University Drive N.W., Calgary, AB T2N 1N4, Canada.

[1]Corresponding author (e-mail: thompson@phas.ucalgary.ca).

1. Introduction

Since its inception, the fundamental principles of electric-quadrupole ion trapping have been explained using the mechanical analogy of a ball contained within a spinning saddle-shaped potential. When the frequency of the spin is controlled correctly, the ball can be prevented from rolling out of the potential (see Fig. 1). Even in his Nobel Prize paper, Paul used this analogy to explain how his traps operated [1]. However, it turns out that this analogy is not entirely qualitatively accurate. Rather than being a rotating electrostatic potential, the Paul-Trap potential is in fact better described as being a "flapping" potential. As time passes, the potential along the x axis oscillates between a trapping well, a field-free region, an anti-trapping potential, and back again. The y-axis potential undergoes a similar oscillation, only 180° out of phase with the x-axis potential (see Fig. 2). In other words, the potential looks remarkably similar to a flapping bird with the potential wings (oriented along the y axis) flapping up and down with time, and the "head and tail" flapping up and down 180° out of phase with the wings. Although qualitatively different in its evolution, the rotating-saddle potential does, in fact, mimic most of the characteristics of the Paul Trap (stability and instability regions, micromotion, and secular oscillation frequency), as will be shown by a theoretical analysis of the motion of a frictionless object in the trap, as well as experimental observations. An analysis, both theoretical and experimental, of the effect of friction is also provided. Experimental measurements were carried out in a rotating-saddle potential that was constructed in the University of Calgary Faculty of Science Machine Shops and has been used in many different presentations and colloquia. However, beyond its use as a teaching aid, the physics of this device is extremely intriguing, leading to a wide range of experimental measurements that have now been carried out to characterize its behaviour.

The goal of this paper is threefold. First, a detailed theoretical analysis of the motion of particles in the kinetic trap is carried out, and the results are compared with the equivalent quantities for the quadrupole ion trap, to quantify how accurate an analogy the kinetic trap is to the ion trap. Second, with the advent of computer-controlled milling machines, the construction of such a potential has become relatively straightforward. However, the published literature on the construction and operation of kinetic traps is limited to one short paper [2]. Therefore, this paper is designed to provide guidance to people interested in constructing such a device, with suggestions on operating parameters and construction tips. Third, this paper outlines the results of a series of experiments related to the stability of objects trapped in the potential and their motion in this trap. In conjunction with these results, some basic theoretical analysis is provided.

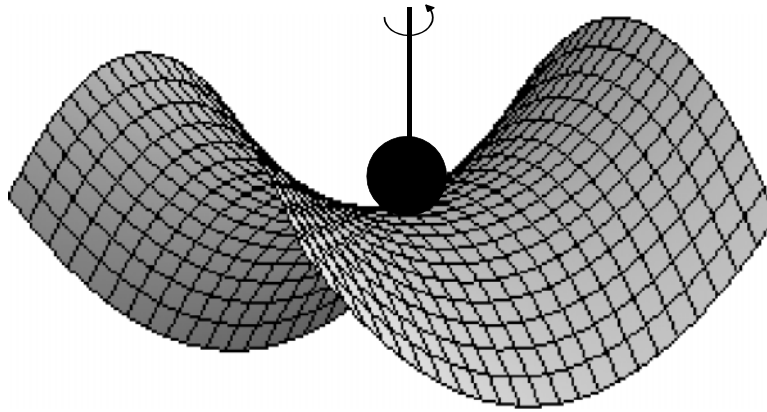## 2. Derivation of electric-quadrupole ion-trapping stability parameters

In the mid 1950s, Paul first demonstrated the operation of a device that could trap and isolate charged particles using pure electric fields. This eventually became known as the Paul Trap, for the development of which he became a Nobel Laureate in 1989. The basic theory of this type of trap is as follows [1,3].

The requirement to trap any object is that it be subject to a restorative force such that when displaced from trap centre in any direction the object is always subject to a force pushing it back to trap centre and increasing with larger displacement from trap centre. The simplest form of such a trapping force is one that increases linearly with displacement from trap centre.

$$\boldsymbol{F} = -c\boldsymbol{r} \tag{1}$$

where $\boldsymbol{F}$ is the force experienced by the object, c is a positive constant, and $\boldsymbol{r}$ is the displacement from trap centre vector.

Since we are looking for a pure electric-trapping field, we need to consider what form of scalar electric potential (ϕ) would generate such a force described by (1). Remembering that the force on a charged particle is proportional to the electric field experienced by the particle, and the electric field is the negative gradient of the electric potential, we can simply integrate (1) to arrive at the desired electric

Fig. 1. Illustration of the time evolution of the potential used for trapping particles via rotating-saddle potentials.

Fig. 2. Illustration of the actual time evolution of the potential used for trapping ions in conventional RF-electric-quadrupole ion traps.

potential

$$\phi(x, y, z) = \frac{\phi_o}{2r_o^2}\left(\alpha x^2 + \beta y^2 + \gamma z^2\right) \tag{2}$$
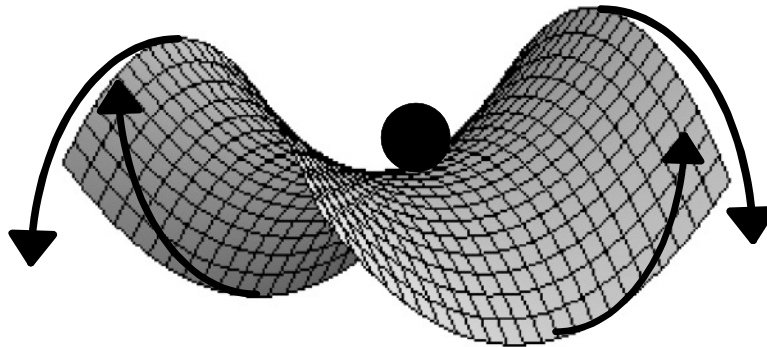
where ϕ_o is a constant defining the magnitude of the potential, r_o is the physical size (radius) of the trap, and α, β, and γ are constant coefficients that determine the shape of the potential. Note that when the integral is carried out, there is a leftover constant of integration, which is effectively determined by the choice of dc-ground in the system. We have, therefore, set this constant of integration to zero. Having a nonzero integration constant has no effect on the following calculations at all since the force is actually proportional to the gradient of the potential and thus this constant would not appear in the force. It is easy to show that taking the negative gradient of (2) results in the required form of (1), so long as

$$\alpha > 0 \tag{3a}$$
$$\beta > 0 \tag{3b}$$
$$\gamma > 0 \tag{3c}$$

However, we are not entirely free to choose our own function for ϕ, since it is an electric potential and thus must satisfy Maxwell's equations. Physically, Gauss's law requires that in free space (no charge density) the integral of the electric field over any closed surface, such as a sphere, must be zero. However, a trapping electric field requires that in all directions the electric-field vectors must point

inwards, clearly violating Gauss's law. Mathematically, Maxwell's equations in free space can be used to produce the following Laplacian equation:

$$\Delta\phi = \nabla \cdot \nabla\phi = 0 \tag{4}$$

Substituting the electric-potential form expressed in (2) into the Maxwell's equations requirement given by (4) results in the following restriction on the coefficients α, β, and γ:

$$\alpha + \beta + \gamma = 0 \tag{5}$$

Clearly it is mathematically impossible to simultaneously satisfy both all of (3) and (5). Thus, it can be categorically stated that a three-dimensional trapping potential cannot be generated by a static electric potential.

The closest that can be achieved is some form of saddle-point potential whereby a trapping field is generated in one or two dimensions and an anti-trapping field is produced in one or two dimensions (Fig. 2). There are two general forms of saddle-point fields commonly used in ion trapping. One is a two-dimensional trapping field with one dimension left field free. This is generated with $\alpha = 1$, $\beta = -1$, and $\gamma = 0$. The other approach is a three-dimensional trapping field that uses $\alpha = \beta = 1$, and $\gamma = -2$.

It may not be clear what use these quadrupole or saddle-point fields are, since clearly the particle has an escape route. However, this discussion has to this point focussed only on static fields, and has not yet considered what can be achieved by allowing the electric field to vary with time. The final basic principle in ion trapping is that at one point in time, the ion is trapped in one direction and starts to escape along a perpendicular direction. However, before it has time to escape, the electric fields reverse so that a trapping field appears along the escape direction to drive the particle back towards trap centre, while the other direction becomes anti-trapping. By repeating this cycle it is possible to hold on to the particle, as long as the correct frequency is chosen. Practically speaking, this is done with ions simply by replacing the static electric field with RF oscillating or ac electric fields.

To quantify the above discussion, we will consider the two-dimensional trapping field described above. The applied, time-varying electric field is given by [4]

$$\Phi(x, y, z, t) = \frac{\Phi_o(t)}{r_o} \left(x^2 - y^2\right) \tag{6}$$

where

$$\Phi_o(t) = U_{DC} + U_{RF} \cos \Omega t \tag{7}$$

Clearly the general applied field has both an ac and a dc component, with U_{DC} giving the amplitude of the dc component, U_{RF} giving the amplitude of the ac component, and Ω providing the angular frequency of oscillation of the ac component. Assuming a symmetric quadrupole trapping field ($U_{DC} = 0$), (6) and (7) combine to yield the time-varying potential of

$$\Phi(x, y, z, t) = \frac{U_{RF}}{r_o} \cos \Omega t \left(x^2 - y^2\right) \tag{8}$$

Applications of Newton's laws and Maxwell's equations yield a pair of differential equations for the motion of the ion in the x–y plane

$$m\frac{d^2}{dt^2}x = -\frac{2eU_{RF}}{r_o^2}\cos(\Omega t)\,x \tag{9a}$$

$$m\frac{d^2}{dt^2}y = -\frac{2eU_{RF}}{r_o^2}\cos(\Omega t)\,y \tag{9b}$$

These equations can be rewritten to the form

$$\frac{d^2}{d\xi^2}x + 2q\cos(2\xi)\,x = 0 \tag{10a}$$

$$\frac{d^2}{d\xi^2}y - 2q\cos(2\xi)\,y = 0 \tag{10b}$$

by the introduction of the unitless coefficients

$$\xi = \frac{\Omega t}{2} \tag{11}$$

$$q = \frac{4eU_{RF}}{mr_o^2\Omega^2} \tag{12}$$

Equations (10a) and (10b) are decoupled differential equations of the form of Mathieu equations. Mathieu equations have been studied extensively since the 19th century. The solutions to these equations fall into one of two distinct classes: stable or bound solutions and unstable or exponentially growing solutions [5]. In the particular case of (10a) and (10b), the largest region of stability is given by the requirement

$$|q| < 0.908\ldots \tag{13}$$

For $|q| > 0.908$, the ion motion grows exponentially, regardless of initial conditions; however, if (13) is satisfied, the ion motion is oscillatory and bounded, also regardless of initial conditions. The motion of the ion is, in fact, made up of two superimposed oscillatory motions. A trapped ion sees a time-averaged pseudo-potential harmonic well due to the trapping field, with its oscillation within this pseudo-well referred to as its secular motion, which is always less than the trap frequency. In addition, the oscillation of the trapping field leads to a superimposed jitter on the secular motion, which is referred to as the micromotion, and the oscillation increases in amplitude as the ion moves further from the trap centre. The micromotion is at the frequency of trapping-field oscillation.

3. Derivation of the rotating-saddle-trap stability parameters

Two modifications are required to adapt ion-trap theory into the theory of the rotating-saddle trap. First, the electric-field potential is replaced with a gravitational potential, and second, the "flapping" potential, described by (8) is replaced by a rotating potential. We will assign the prime frame as the rotating frame fixed to the potential. In this frame, the gravitational potential is given by

$$U(x', y') = \frac{mgh_o}{r_o^2}\left(x'^2 - y'^2\right) \tag{14}$$

where r_o is the radius of the rotating saddle, and h_o is the maximum height of the saddle at the radius r_o, measured relative to the height of the middle of the trap. Note that this is a symmetric potential and, thus, it is mimicking the symmetric Paul Trap ($U_{RF} = 0$). Converting this potential to the laboratory frame, it becomes

$$U(x, y) = \frac{mgh_o}{r_o^2}\left[\left(x^2 - y^2\right)\cos(2\Omega t) + 2xy\sin(2\Omega t)\right] \tag{15}$$

where Ω is the rotation frequency of the trap. This form of the potential clearly shows the quantitative mathematical difference between the flapping Paul-Trap potential ((8)) and the rotating-saddle potential. This difference is simply the additional sine term seen on the right-hand side in (15). Practically, this

additional term means that the potential is always present and of the same amplitude, as opposed to the Paul-Trap potential, which has zero amplitude whenever $\Omega t = (2n + 1)\pi$ (n = integer). Although this additional term would seem to increase the complexity of the problem relative to the Paul-Trap potential, especially since it converts the problem from one of two decoupled differential equations to one with coupled differential equations, in point of fact, we will show that this additional term allows for an exact solution to this problem.

The next step is to use Newton's laws to generate a pair of coupled linear differential equations to govern the motion of the ball bearing in the x–y plane. Using $\boldsymbol{F} = -\boldsymbol{\nabla}U$ we find

$$m\frac{\partial^2}{\partial t^2}x = \frac{2mgh_{\mathrm{o}}}{r_{\mathrm{o}}^2}\left[-x\cos(2\Omega t) - y\sin(2\Omega t)\right] \tag{16a}$$

$$m\frac{\partial^2}{\partial t^2}y = \frac{2mgh_{\mathrm{o}}}{r_{\mathrm{o}}^2}\left[y\cos(2\Omega t) - x\sin(2\Omega t)\right] \tag{16b}$$

As with the quadrupole ion-trap theory, we will now again convert to unitless parameters by defining

$$\tau = \Omega t \tag{17}$$

$$\bar{q} = \frac{gh_{\mathrm{o}}}{r_{\mathrm{o}}^2\Omega^2} \tag{18}$$

Note that the unitless time parameter τ for this case differs from the ξ coefficient in the previous section by a factor of 2. This is due to the symmetry of the saddle potential. Whereas in the flapping ion-trap potential, it returns to its $t = 0$ form only when $\Omega t = 2\pi n$ (n = integer), the rotating saddle is identical to its $t = 0$ state at $\Omega t = \pi n$. Thus, from the point of view of the trapped particle, for a given angular frequency Ω, the rotating-saddle trap appears to cycle twice as fast as the quadrupolar oscillating trap. In addition, since we are using gravity to produce the trapping force, the mass of the trapped particle cancels out leaving a trapping coefficient $\bar{q}$ that has the same frequency, trap size, and trap depth dependences as the ion trap q, but a generally simpler form. With these definitions, (16a) and (16b) become

$$\frac{\partial^2}{\partial\tau^2}x + 2\bar{q}\left[x\cos(2\tau) + y\sin(2\tau)\right] = 0 \tag{19a}$$

$$\frac{\partial^2}{\partial\tau^2}y - 2\bar{q}\left[y\cos(2\tau) - x\sin(2\tau)\right] = 0 \tag{19b}$$

Comparing (19) with the ion-trap equivalent (10), we see that they have almost identical form, other than the sinusoidal cross-coupling term. To deal with this term, we will work in the complex plane ($z = x + iy$), which allows us to reduce this pair of coupled differential equations to a single, analytically soluble, complex differential equation. To do this we simply add (19a) to $i \times$ (19b), and defining $z = x + iy$ we can rearrange the resulting equation to get

$$\frac{\partial^2}{\partial\tau^2}z + 2\bar{q}z^*\mathrm{e}^{i2\tau} = 0 \tag{20}$$

To solve this complex differential equation, we carry out a similar substitution to that used in atomic and optical quantum mechanics problems (for example, see ref. 6) in the rotating-wave approximation [7]. A new time-dependent function $f(\tau)$ is defined by

$$z(\tau) = f(\tau)\,\mathrm{e}^{i\tau} \tag{21}$$

Substituting (21) (and its second derivative) into (20) and cancelling a common factor of $\mathrm{e}^{i\tau}$ yields

$$\frac{\mathrm{d}^2}{\mathrm{d}\tau^2}f(\tau) + 2i\frac{\mathrm{d}}{\mathrm{d}\tau}f(\tau) - f(\tau) + 2\bar{q}f^*(\tau) = 0 \tag{22}$$

To produce an equation in terms of only $f(\tau)$ and not $f^*(\tau)$, we simply take the complex conjugate of (22), and then use (22) to eliminate $f^*(\tau)$ and all of its derivatives from our new equation, this yields the fourth-order differential equation

$$f^{(4)}(\tau) + 2f^{(2)}(\tau) + \left(1 - 4\bar{q}^2\right) f(\tau) = 0 \tag{23}$$

The solution to this differential equation is the sum of four independent complex exponential terms of the form

$$f(\tau) = A\,e^{+\beta_+\tau} + B\,e^{-\beta_+\tau} + C\,e^{+\beta_-\tau} + D\,e^{-\beta_-\tau} \tag{24a}$$

with the $\beta_\pm$ coefficients given by

$$\beta_\pm = \sqrt{\pm 2|\bar{q}| - 1} \tag{25}$$

The weighting of each exponential is determined from the initial conditions. If all of the β_i coefficients are purely imaginary, then the particle evolution is bounded. However, the existence of nonzero real components of the coefficients results in at least one exponentially growing term that evolves to infinity at large times, corresponding to a non-trapped particle. Clearly, all coefficients will be purely complex if and only if

$$2|\bar{q}| \le 1 \tag{26}$$

or, choosing h_o and r_o to be positive constants

$$2\bar{q} = \frac{2gh_o}{\Omega^2 r_o^2} \le 1 \tag{27}$$

which means that this is the trapping condition, equivalent to (13) in the previous section, only in this case it could be determined analytically.

Note that, like the RF-quadrupole ion trap, theoretical stability or instability is virtually independent of the initial conditions of the trapped particle, dependent only on the value of the trapping coefficient q. The sole exception to this statement is the case of initial conditions $\boldsymbol{r} = \boldsymbol{v} = 0$ where the trapped particle is initially stationary exactly at the centre of the trap. Under these conditions, the particle will remain trapped at trap centre regardless of the value of the q coefficient. This result was confirmed in the laboratory (see Sect. 4), when occasionally the ball bearing would start at the exact centre of the rotating potential resulting in very stable and long-lasting trapped-particle behaviour.

Finally, a small amount of linear algebra is necessary to produce a general analytical expression for the evolution of a trapped object based on its initial position and velocity as well as the trapping parameter $\bar{q}$. Given an initial position $z(0) = f(0) = z_o$, and an initial velocity $\frac{dz(0)}{d\tau} = v_o$ $(\frac{df(0)}{d\tau} = \boldsymbol{v} = v_o - iz_o)$, we can solve for the coefficients A, B, C, and D. To provide four equations for the four unknowns we employ (22) to calculate the initial values of the second and third temporal derivatives of $f(\tau)$ based on the initial position and velocity. In carrying out this calculation we will define

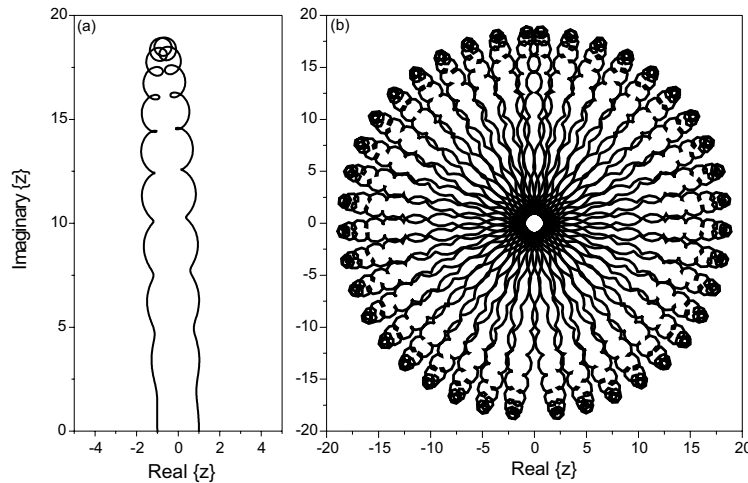$$\beta_\pm = i\mu_\pm, \qquad \mu_\pm = \sqrt{1 \mp 2|\bar{q}|} \tag{28}$$

where $\mu_\pm$ are real for trapped-particle conditions. With this substitution, (24a) becomes

$$f(\tau) = A\,e^{+i\mu_+\tau} + B\,e^{-i\mu_+\tau} + C\,e^{+i\mu_-\tau} + D\,e^{-i\mu_-\tau} \tag{24b}$$

and the initial conditions yield a set of four independent linear equations

$$A + B + C + D = z_o \tag{29}$$

Fig. 3. Theoretical trajectory for a particle trapped in a low-$\bar{q}$ potential ($\bar{q} = 0.05$) with initial conditions $f(0) = 1$, $\frac{d}{d\tau} f(0) = 0$: (*a*) illustrates the evolution from $\tau = 0$ to 53 demonstrating the micromotion and secular motion and (*b*) illustrates the evolution from $\tau = 0$ to 2513 to demonstrate the precession of the orbit.

$$i\mu_+(A - B) + i\mu_-(C - D) = v_{\mathrm{o}} - iz_{\mathrm{o}} \tag{30}$$

$$-\mu_+^2(A + B) - \mu_-^2(C + D) = -2iv_{\mathrm{o}} - z_{\mathrm{o}} - 2\bar{q}z_{\mathrm{o}}^* \tag{31}$$

$$-i\mu_+^3(A - B) - i\mu_-^3(C - D) = -3v_{\mathrm{o}} - 2\bar{q}v_{\mathrm{o}}^* + iz_{\mathrm{o}} + 2i\bar{q}z_{\mathrm{o}}^* \tag{32}$$

These inhomogeneous linear equations can be solved for given values of $\bar{q}$, z_{o}, and v_{o}. Figures 3–5 are examples of the results of such a calculation illustrating that the motion of a trapped particle is quite similar to the motion of the trapped ion. At low values of $\bar{q}$ (Fig. 3) we see the same separation of motion into a high-frequency micromotion at the trap frequency (resulting from the $e^{i\tau} = e^{i\Omega t}$ factor in (21)), superimposed on the slower secular oscillation in the time-averaged pseudo-potential, just like that seen with trapped ions. At low-trapping parameters $\bar{q}$, this secular motion occurs at $\bar{q}\Omega$, and in Fig. 3*b* we also see an even slower precession in the orbits at frequency $\bar{q}^2\Omega$.

This simple formula for the secular frequency holds only for low values of $\bar{q}$ and can be derived based on a time-averaged pseudo-potential approach in which the potential is averaged over a period of the saddle-potential rotation to produce an average potential well (see pp. 210–212 of ref. 3) experienced by the ion. In this approach, valid only for small $\bar{q}$ where the micromotion and secular-motion frequencies are well separated, we break the particle motion down into two components

$$z = Z + \delta \tag{33}$$

where Z is the secular motion and δ is the micromotion. The micromotion amplitude tends to be much smaller than the secular motion amplitude ($\delta << Z$) but given its higher frequency of oscillation, its temporal derivatives tend to be larger ($\ddot{\delta} >> \ddot{Z}$). In this limit, (20) takes the form

$$\ddot{Z} + \ddot{\delta} = -2\bar{q}(Z^* + \delta^*)\, e^{i2\tau} \tag{34}$$

while neglecting the smaller terms reduces this to

$$\ddot{\delta} = -2\bar{q}Z^*\, e^{i2\tau} \tag{35}$$

Equation (35) can be solved to express δ in terms of Z by taking Z to be a constant, since it varies slowly on the time scale of δ, and integrating twice to produce

$$\delta = \frac{1}{2}\bar{q}Z^*\, e^{i2\tau} \tag{36}$$

Fig. 4. Observed secular-motion frequency for theoretical trapped-particle trajectories as a function of the trapping parameter $\bar{q}$. The function for the continuous line is the theoretically predicted relation for low values of $\bar{q}$.
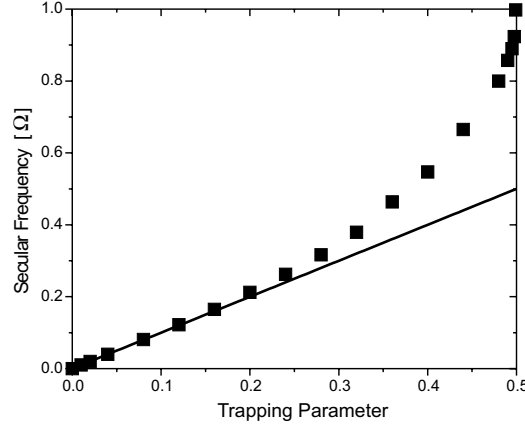
Substituting (36) back into (33) produces a first-order expression for z in terms of Z alone

$$z = Z + \frac{1}{2}\bar{q}Z^*\,e^{i2\tau} \tag{37a}$$

$$z^* = Z^* + \frac{1}{2}\bar{q}Z\,e^{-i2\tau} \tag{37b}$$

Substituting expression (33) into the left-hand side of (20) and (37b) into the right-hand side yields

$$\ddot{Z} + \ddot{\delta} = -2\bar{q}Z^*\,e^{i2\tau} - \bar{q}^2 Z \tag{38}$$

Finally, we average (38) over one trap cycle. Z, which varies slowly, takes on an averaged value $\langle Z \rangle$, while $\langle \ddot{\delta} \rangle = 0$ because the micromotion has the period of one trap cycle and $\langle 2\bar{q}Z^*e^{i2\tau} \rangle \cong 0$ because Z^* oscillates very slowly on this time scale and the exponential averages to zero. Thus, (38) reduces to

$$\langle \ddot{Z} \rangle = -\bar{q}^2 \langle Z \rangle \tag{39}$$

converting back to derivatives with respect to time t yields

$$\frac{d^2}{dt^2}\langle Z \rangle = -\bar{q}^2 \Omega^2 \langle Z \rangle \tag{40}$$

which is clearly just the equation for a harmonic oscillator of frequency $\bar{q}\Omega$. Therefore, for small values of $\bar{q}$, the position of the particle averaged over one trap period (the definition of secular motion) should oscillate at frequency $\bar{q}\Omega$, as observed. Note that the time-averaged pseudo-potential is simultaneously trapping in both x and y dimensions, thus allowing this trap to hold a particle as long as its secular frequency does not exceed the trap-rotation frequency, at which point the particle no longer sees the averaged potential. The equivalent calculation for the low-q dependence of the secular frequency of RF-electric quadrupole trapped ions is $\omega_{\text{sec}} = \frac{1}{\sqrt{8}}q\Omega$ [8].

Figure 4 provides the results of computationally determining the secular frequency for different values of $\bar{q}$ (with the same initial conditions). We clearly see that as $\bar{q}$ significantly exceeds 0.15 the $\omega_{\text{sec}} = \bar{q}\Omega$ relation (continuous line) begins to fail, as expected, since the above approximations begin to fail. Figure 4 also illustrates an interesting physical explanation for the instability limit. We clearly see that the secular frequency approaches the trap frequency as we approach the stability limit, and that

Fig. 5. Theoretical trajectory for a particle trapped in a high-$\bar{q}$ potential ($\bar{q} = 0.375$) with initial conditions $f(0) = 1$, $\frac{d}{d\tau} f(0) = 0$. The particle evolution covers the time period $\tau = 0$ to 38.
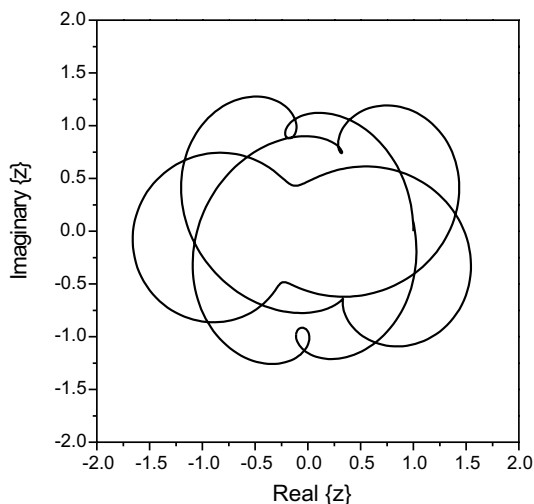
Fig. 6. Theoretical trajectory for a particle expelled from a high-$\bar{q}$ non-trapping potential ($\bar{q} = 0.501$) with initial conditions $f(0) = 1$, $\frac{d}{d\tau} f(0) = 0$.
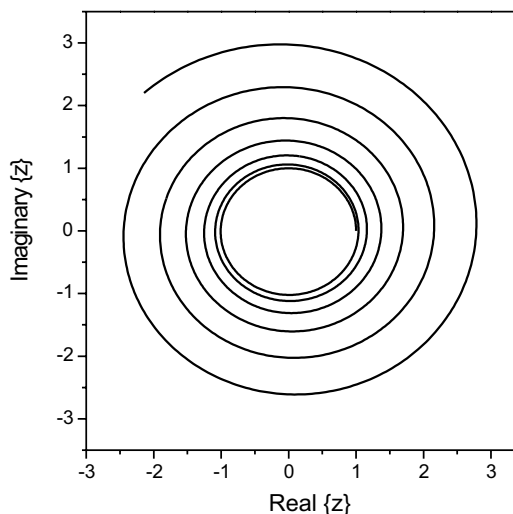
the particle becomes unstable when the frequency of its oscillation exceeds the frequency at which the potential rotates. In other words, under unstable conditions, the particle can escape the trap before the potential has time to rotate and drive the particle back towards trap centre.

Figure 5 illustrates the motion of a trapped particle with a larger value of $\bar{q}$, although still less than 0.5. For these larger values of $\bar{q}$, the secular and micromotion frequencies become comparable, and thus we no longer have clearly defined micromotion and secular-motion components in the plots. The system constructed in Calgary was only capable of operation at these higher $\bar{q}$ values, and the cusp-like behaviour illustrated in Fig. 5 was one of the noticeable characteristics of the trapped-particle motion in the Calgary trap (see Sect. 4). Finally, Fig. 6 illustrates what happens if $\bar{q}$ exceeds 0.5, rapid exponential growth in the motion illustrating non-bounded motion.

With the theoretical and computational basis of the rotating-saddle trap well-established, it was time to move on to the construction of such a device.

4. Practical rotating-saddle trap and lifetime tests

Once the stability regime had been determined, it was possible to design and build a practical rotating-saddle potential for trapping stainless-steel ball bearings. After some trial and error, it was determined that a trap-rotation frequency in the neighbourhood of 1 Hz would be a good choice. Deeper traps (larger h_o for the same r_o), which would require a higher rotation speed, were less than ideal for two safety reasons. First, the higher walls and faster rotation speed made it dangerous to manually insert the ball bearing into the trap. In addition, the speed at which a ball bearing in the trap moves in the laboratory frame is proportional to the rotation speed of the trap. Therefore, higher speed traps produce dangerously fast-moving ball bearings when they escape the trapping area.

For these reasons, the trap built at the University of Calgary had technical parameters of $2r_o = 150$ mm and $2h_o = 25$ mm. These quantities inserted in (27) yield a frequency range for stable trapping of $\Omega > 2\pi$ (1.05 Hz).

Figure 7 shows a photograph of the Calgary apparatus. The saddle was made out of clear acrylic, allowing it to be used on an overhead projector for larger group demonstrations, machined out of a solid cylinder using a CAD-controlled computerized milling machine. The saddle was placed in a bearing

Fig. 7. Photograph of the rotating-saddle trap apparatus illustrating the storage of a large ball bearing at a rotational rate slightly above 2π s^{-1}.
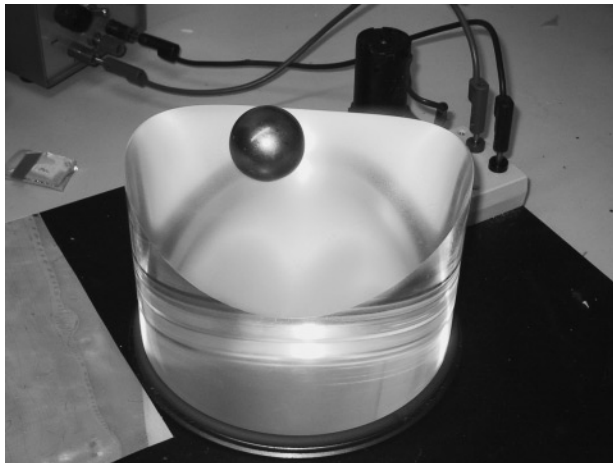
Fig. 8. Plot of average trapped-ion lifetime versus trap-rotation frequency for a non-Teflon-coated ball bearing in a rotating-saddle potential. The saddle dimensions are those given in the text. The vertical broken line illustrates the theoretical frequency threshold for bounded motion in the rotating-saddle potential.
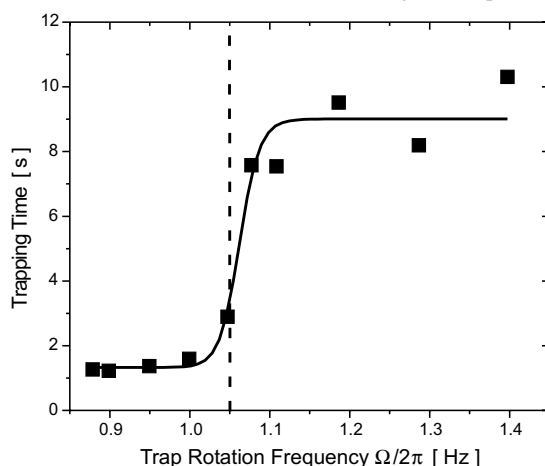
ring mounted in a stainless-steel base. A simple DC motor was used to drive the rotation through a rubber o-ring drive assembly with a "gear ratio" selected such that 1 Hz rotation was achieved with a driving voltage on the motor of slightly over 40 V$_{dc}$. The system could be operated up to approximately 50 V$_{dc}$ without damaging the electronics. The trap-rotation frequency was measured by placing a small mirror on the side of the saddle potential. A HeNe laser was then reflected off the mirror to a small photodiode. As the saddle rotated the photodiode gave off electrical pulses separated by the period of rotation.

The lifetime of a steel ball bearing in the trap was then measured as a function of trap-rotation speed with the results shown in Fig. 8. These clearly show a step increase of roughly a factor of 10 occurring very near to 1.05 Hz, as predicted by theory. However, this increase does not reach the infinite lifetimes predicted by the frictionless particle theory. Clearly something is missing from the model, and just as clearly, this something is friction.

5. The effect of friction

Quantifying the effect of friction in the laboratory is difficult. However, a qualitative experiment in which the trapped ball bearing was sprayed with a Teflon lubricant coating resulted in an increase in the trapping time by between 1 and 2 orders of magnitude. This confirmed experimentally that friction is a major cause of the limitations in the trap lifetime.

This effect can be confirmed theoretically by introduction of a frictional force due to the trapped particle moving relative to the surface of the rotating-saddle potential. In the laboratory frame, this force takes the form (α is the real, positive friction coefficient)

$$F_{\text{friction}} = -\alpha \left(\frac{\mathrm{d}}{\mathrm{d}t} z(t) - i\Omega z(t) \right) = -\alpha\Omega \left(\frac{\mathrm{d}}{\mathrm{d}\tau} z(\tau) - iz(\tau) \right) \tag{41}$$

where the second term in the expression is due to the rotation of the saddle potential surface. Substituting this term into the left-hand side of (20) yields (defining $\bar{\alpha} = \alpha/(m\Omega)$)

$$\frac{\mathrm{d}^2}{\mathrm{d}\tau^2} z + 2\bar{q}z^* \mathrm{e}^{i2\tau} = -\bar{\alpha} \left(\frac{\mathrm{d}}{\mathrm{d}\tau} z - iz \right)$$

$$\frac{\mathrm{d}^2}{\mathrm{d}\tau^2} z + \bar{\alpha} \left(\frac{\mathrm{d}}{\mathrm{d}\tau} z - iz \right) + 2\bar{q}z^* \mathrm{e}^{i2\tau} = 0 \tag{42}$$

Carrying out the usual substitution for z ((21)) yields the constant coefficient differential equation

$$\frac{\mathrm{d}^2}{\mathrm{d}\tau^2} f(\tau) + (\bar{\alpha} + 2i) \frac{\mathrm{d}}{\mathrm{d}\tau} f(\tau) - f(\tau) + 2\bar{q} f^*(\tau) = 0 \tag{43}$$

Comparing (43) with (22), we see that we have simply picked up a real part in the coefficient of the $\frac{\mathrm{d}}{\mathrm{d}\tau} f(\tau)$ term. This conversion of the coefficient from purely imaginary to complex results in the general solutions having complex exponential coefficients (unstable orbits), rather than the purely real or imaginary exponential coefficients of the friction-free case. Re-expressing this as a single differential in $f(\tau)$ (equivalent to (23)) yields

$$f^{(4)}(\tau) + 2\bar{\alpha} f^{(3)}(\tau) + (2 + \bar{\alpha}^2) f^{(2)}(\tau) - 2\bar{\alpha} f^{(1)}(\tau) + \left(1 - 4\bar{q}^2 \right) f(\tau) = 0 \tag{44}$$

Equation (44) can be converted to a fourth-order polynomial by the substitution of exponential solutions of the form $f(\tau) = \mathrm{e}^{\beta\tau}$

$$\beta^4 + 2\bar{\alpha}\beta^3 + (2 + \bar{\alpha}^2)\beta^2 - 2\bar{\alpha}\beta + \left(1 - 4\bar{q}^2 \right) = 0 \tag{45}$$

As a somewhat messy fourth-order polynomial, we cannot write down a general solution for β. However, for small $\bar{\alpha}$, we can solve this polynomial by assuming that β is simply the friction-free solutions $\beta_\pm$ plus a small correction term $\sigma_\pm$. Substituting $\beta = \beta_\pm + \sigma_\pm$ into (45), and keeping only terms up to first order in the small quantities $\bar{\alpha}$ and (or) σ yields

$$\beta_\pm^4 + 4\beta_\pm^3\sigma_\pm + 2\bar{\alpha}\beta_\pm^3 + 2\beta_\pm^2 + 4\beta_\pm\sigma_\pm - 2\bar{\alpha}\beta_\pm + \left(1 - 4\bar{q}^2 \right) = 0 \tag{46}$$

From (25), $\beta_\pm = \sqrt{\pm 2|\bar{q}| - 1}$; substituting this into (46) results in the first, fourth, and last terms cancelling each other and leaving

$$4\beta_\pm^3\sigma_\pm + 2\bar{\alpha}\beta_\pm^3 + 4\beta_\pm\sigma_\pm - 2\bar{\alpha}\beta_\pm = 0 \tag{47}$$

which has the solution

$$\sigma_\pm = \frac{1 - \beta_\pm^2}{2(1 + \beta_\pm^2)}\bar{\alpha} = \pm\tfrac{1}{2\bar{q}}(1 \mp \bar{q})\bar{\alpha} \tag{48}$$

The correction factor given by (48) is clearly always real and proportional to $\bar{\alpha}$, and thus, at least two of the terms in the solution of the form of (24a) will grow exponentially with time leading to a finite particle lifetime in the trap, as long as $\bar{\alpha}$ is nonzero.

6. Effect of initial conditions

In the previous section it was stated that the stability of the trap system is independent of initial conditions. Although this is true, the trapping lifetime is very sensitive to initial conditions, with increased lifetimes resulting from starting the particle at rest closer to the centre of the potential. This effect has been observed in the laboratory. Theoretically, this can be explained by the fact that either due to friction or to selection of an unstable trapping parameter, the orbit of the particle grows exponentially (see Fig. 6). If we label the radius of the starting point of the particle by R and the radius of the trapping potential by r_o, the trap lifetime T_L is given by the expression

$$r_o = R\,e^{\beta\Omega T_L} \quad \text{or} \quad R = r_o\,e^{-\beta\Omega T_L} \tag{49a}$$

$$T_L = \frac{1}{\beta\Omega}\ln\left(\frac{r_o}{R}\right) \tag{49b}$$

where for $\bar{q} > 0.5$, we can replace β with $\beta_+ = \sqrt{2\bar{q} - 1}$, while for stable trapping parameters, β is proportional to the friction coefficient α (for small α).

This analysis can be taken a step further if we assume that the initial placement distribution is given by a two-dimensional Gaussian centred on the middle of the trap. The probability density of placing the particle at a given initial radius R is then given by

$$P(R) = CR\,e^{-(R/a)^2} \tag{50}$$

where C is a normalization constant and a gives the width of the distribution. We can now calculate the probability of observing a given lifetime using $P(T_L) = P(R)\left|\frac{dR}{dT_L}\right|$, to get

$$P(T_L) = Cr_o^2\Omega\beta\,e^{-2\beta\Omega T_L}\,\exp\left[-\left(\frac{r_o}{a}\right)^2\,e^{-2\beta\Omega T_L}\right] \tag{51}$$

This is a somewhat complex function, but in fact it is determined by three variables: $C\,r_o^2\,\Omega$ (normalization term), β (friction/unstable trapping term), and r_o/a (distribution width). The latter two coefficients provide physically significant results, providing information about the trap behaviour and the accuracy of the initial position, respectively. The overall normalization or scaling factor is less useful.

This model can be tested without actually measuring the initial position. Instead, the lifetime of a trapped particle was measured 25 to 30 times for a given trapping-parameter value. The distribution of lifetimes was then fit to function (51). Figure 9 illustrates typical data for this type of experiment. No tests with very short lifetimes are observed because it takes a finite time for the ball to travel to the edge of the trap. There is then a peak in the temporal spectrum whose width and maximum is determined by the trapping parameters and is principally fit using (51). The data for Fig. 9 were collected with a non-trapping coefficient value of $\bar{q} = 0.712$ (trap-rotation frequency $\Omega = 2\pi(0.88\text{ Hz})$). By choosing this low a trap frequency, we can estimate $\beta = \beta_+ = \sqrt{2|\bar{q}| - 1} = 0.65$. Interestingly the $(r_o/a)^2$ coefficient for the fit to these data is 3300, corresponding to a value of $a = 1.3$ mm, which seems to be a quite reasonable value for the accuracy of manual loading of a particle into the trap. Occasionally, very

Fig. 9. Plot of number of observations versus observed lifetime for ions placed in a rotating-saddle potential with trapping parameter $\bar{q} = 0.712$. The continuous line fit function is described in the main text.
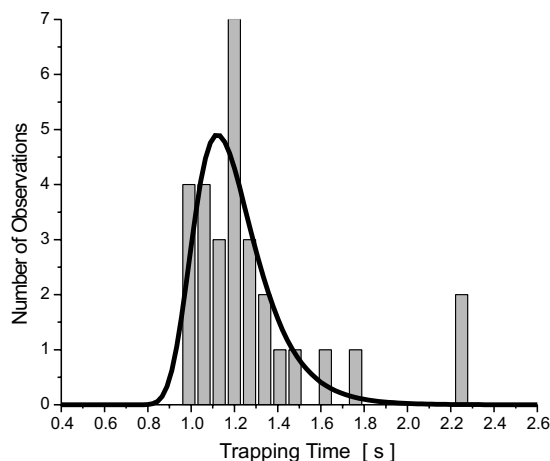
long trap lifetimes are observed when the ball starts very close to the trap centre, resulting in this case in the peak near 2.25 s. However, these long lifetime "peaks" result from the statistics of small numbers and are not quantitatively repeatable. They tend to occur in most data sets, but their exact location is quite variable.

7. The rotating-saddle trap and physics education

The rotating-saddle trap is an excellent mechanical analogy for illustrating the operating principles of quadrupole ion trapping. However, its physics education uses go far beyond a simple lecture demonstration.

From the theoretical and computational physics point of view, this physical system is analytically solvable using techniques very similar to those employed in the rotating-wave approximation and quantum mechanical interaction picture techniques of atomic physics and quantum optics [6,7]. By first tackling calculations in rotating bases in this type of mechanical system, it may help many students understand what they are doing when asked to carry out similar techniques in the more abstract areas of quantum mechanics. From the computational point of view, this provides a system of coupled differential equations with time-varying coefficients that is analytically solvable. Thus, students can hone their computational skills and tools by solving this system numerically and comparing their results to the analytical solutions. In addition, as shown in the previous section, this system provides some useful insight into statistical physics.

From the experimental physics teaching laboratory point of view, this is a wonderful apparatus. Not only does it provide students with the chance to directly observe and experiment with particle trapping to a degree not possible with conventional atom and ion trapping systems, should such systems ever be affordable for a teaching laboratory, but the apparatus is inherently safe both from the point of view of students damaging the equipment and vice versa. Students carrying out projects in an experimental methods course collected all of the experimental data presented in this work. The students were given a basic introduction to the apparatus, including a short discussion about some interesting features, and then they were allowed to develop their own experimental method to carry out measurements of some property of the system. As an added benefit, it is possible to carry out calculations to compare theory with many of the measurements. However, it is the ability to let students explore this apparatus independently, allowing each student to have a unique experience, that makes it such a good candidate for a senior level undergraduate teaching laboratory project.

Fig. 10. Plot of average trapping time (6 trial average) for a Teflon-coated ball bearing versus saddle-potential tilt angle relative to the vertical. The continuous line is included simply as a guide to the eye.
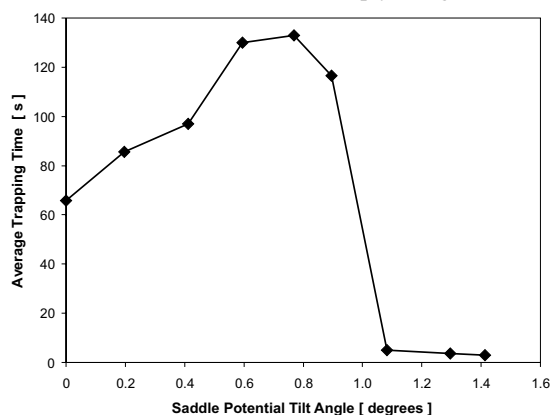
8. Future directions

It is expected that this apparatus will be integrated into the University of Calgary Senior Teaching Laboratory as a Particle Trapping Laboratory in the near future. From a technical point of view, one of the future goals will be to develop an imaging system (stroboscopic, video, or long-exposure imaging) to allow quantitative comparison between experimental and theoretical particle orbits. Related to this, the present saddle potential is too deep to allow easy experimental access to the low-$\bar{q}$ ($\bar{q} < 0.1$) regime where the micromotion and secular motion degrees of freedom are well separated. Therefore, it is hoped that a new shallower saddle potential can be built in the future. In addition, future student experimental method projects may include studying multiple trapped particles and the effect of collisions on trapping and heating.

From the computational/theoretical perspective, future student projects may include comparison of the analytical results for basic trap operation with various computational techniques for solving time-dependent differential equations. A more complicated problem is that of saddle tilt, somewhat equivalent to homogeneous versus inhomogeneous field trapping in ion traps. In a recent experiment, trap lifetimes for a Teflon-lubricated particle were measured as a function of the tilt angle of the trap (determined by reflecting a HeNe laser off a mirror sheet attached to the trap base plate). Unexpectedly the trap lifetime increased by roughly a factor of 2 for a tilt angle of just under 1° (see Fig. 10) regardless of whether the trap was tilted forward or backward. In the future, student projects may include attempting to model this effect theoretically or computationally, as well as examining this effect as a function of the trapping parameter.

9. Conclusions

The rotating-saddle potential trap provides an excellent mechanical analogy for demonstrating the concepts and principles of RF-electric quadrupole ion trapping. The theory of rotating-saddle trapping largely mirrors that of ion trapping, with slight differences that have the added benefit of making the problem analytically solvable, thus making this an interesting physical system to study experimentally and theoretically. The predictions of the theory were shown to match those of an actual rotating ball-bearing trap constructed and tested at the University of Calgary. The prediction of stable trap behaviour was shown to be quantitatively accurate, while the observed periodic motion of the particles was in good qualitative agreement with theory. It has been observed experimentally and confirmed theoretically that friction has a fundamental effect on trap lifetime, with only friction-free traps being capable of infinitely long trapping periods. The statistical effect of randomization of initial conditions on trap lifetime were observed and modelled as well. Finally, the wide range of applications of this apparatus to teaching

trapped-particle physics as well as other more general physical principles were outlined, and a discussion of future directions was included. It is hoped that this document will encourage other physics departments to consider the benefits of employing rotating-saddle traps as an integral part of their senior teaching laboratories.

Acknowledgements

References

1. W. Paul. *In* Electromagnetic traps for charged and neutral particles. Laser manipulation of atoms and ions. Proceedings from the International School of Physics Enrico Fermi. 9–19 July 1991, Varenna, Italy. *Edited by* E. Arimondo, W. Phillips, and F. Strumia. North-Holland, Amsterdam, New York. 1992. pp. 497–517.
2. W. Rueckner, J. Georgi, D. Goodale, D. Rosenberg, and D. Tavilla. Am. J. Phys. **63**(2), 186 (1995).
3. P.H. Dawson. *In* Quadrupole mass spectrometry and its applications. *Edited by* P.H. Dawson. Elsevier Scientific Publishing Company, Amsterdam. 1976. pp. 9–92.
4. R.E. March and R.J. Hughes. Quadrupole storage mass spectrometry. John Wiley and Sons, New York. 1989.
5. F.M. Arscott. Periodic differential equations: an introduction to Mathieu, Lamé, and allied functions. MacMillan, New York. 1964.
6. S.E. Harris, J.E. Field, and A. Imamoglu. Phys. Rev. Lett. **64**, 1107 (1990); R.I. Thompson, B.P. Stoicheff, G.Z. Zhang, and K. Hakuta. Appl. Phys. B, **60**, S129 (1995).
7. R.W. Boyd. Nonlinear optics. Academic Press, Boston. 1992. p. 199.
8. M. Welling, H.A. Schuessler, R.I. Thompson, and H. Walther. Intl. J. Mass Spectrom. Ion Proc. **172**, 95 (1998).